Title

JMJD8 is a Novel Molecular Nexus Between Adipocyte-Intrinsic Inflammation and Insulin Resistance.

Journal

Diabetes, 71(1)

Authors

You, Dongjoo

Chul Jung, Byung

Villivalam, Sneha

et al.

Publication Date

2021-10-22

DOI

10.2337/db21-0596

Peer reviewed

JMJD8 Is a Novel Molecular Nexus Between Adipocyte-Intrinsic Inflammation and Insulin Resistance

Dongjoo You,[1] Byung Chul Jung,[1] Sneha Damal Villivalam,[1] Hee-Woong Lim,[2] and Sona Kang[1]

Diabetes 2022;71:43–59 | https://doi.org/10.2337/db21-0596

Chronic low-grade inflammation, often referred to as metainflammation, develops in response to overnutrition and is a major player in the regulation of insulin sensitivity. While many studies have investigated adipose tissue inflammation from the perspective of the immune cell compartment, little is known about how adipocytes intrinsically contribute to metainflammation and insulin resistance at the molecular level. In this study, we demonstrate a novel role for Jumonji C domain-containing protein 8 (JMJD8) as an adipocyte-intrinsic molecular nexus between inflammation and insulin resistance. We determined that JMJD8 was highly enriched in white adipose tissue, especially in the adipocyte fraction. Adipose JMJD8 levels were dramatically increased in obesity-associated insulin resistance models. Its levels were increased by feeding and insulin and inhibited by fasting. A JMJD8 gain-of-function was sufficient to drive insulin resistance, whereas loss-of-function improved insulin sensitivity in mouse and human adipocytes. Consistent with this, *Jmjd8*-ablated mice had increased whole-body and adipose insulin sensitivity and glucose tolerance on both chow and a high-fat diet, while adipocyte-specific *Jmjd8*-overexpressing mice displayed worsened whole-body metabolism on a high-fat diet. We found that JMJD8 affected the transcriptional regulation of inflammatory genes. In particular, it was required for lipopolysaccharide-mediated inflammation and insulin resistance in adipocytes. For this, JMJD8 required interferon regulatory factor 3 to mediate its actions in adipocytes. Together, our results demonstrate that JMJD8 acts as a novel molecular factor that drives adipocyte inflammation in conjunction with insulin sensitivity.

Chronic, low-grade tissue and systemic inflammation have been proposed as major mechanisms for insulin resistance in obesity (1–3). Adipose tissue stands at this nexus between inflammation and metabolism (2). In the lean state, leukocytes interact with macrophages within the adipose tissue to maintain low inflammatory tone and appropriate insulin sensitivity (3,4). However, during chronic overnutrition, there are fewer anti-inflammatory immune cells (e.g., eosinophils, innate lymphoid type 1 and 2 cells, and regulatory T cells) (5–9) and increased infiltration of proinflammatory immune cells (e.g., M1 macrophages, B cells, Th1 and 17 cells, dendritic cells, and neutrophils) (10–16). Concordantly, there is a concomitant decrease in local and circulating levels of anti-inflammatory cytokines, such as interleukin-4 (IL-4) and IL-13 (5–9), and increased levels of proinflammatory cytokines and chemokines, such as tumor necrosis factor-α (TNF-α) (17,18) and IL-6 (14), which trigger innate immune signaling and are commonly associated with insulin resistance.

It has been proposed that this inflammation is reacting to lipopolysaccharide (LPS), which is an outer membrane component of Gram-negative bacterial cell walls. High-fat diets (HFDs) may alter the gut microbiome and intestinal wall permeability, increasing enterobacterial production and LPS translocation into systemic circulation (19). Indeed, some groups of obese subjects and subjects with type 2 diabetes (T2D) (20,21) have elevated LPS plasma concentrations. In addition, an HFD increases the LPS concentrations in circulation in both healthy subjects and those with T2D (20,22), and LPS administration to

[1]Nutritional Sciences and Toxicology Department, University of California Berkeley, Berkeley, CA
[2]Division of Biomedical Informatics, Department of Pediatrics, Cincinnati Children's Hospital Medical Center, University of Cincinnati College of Medicine, Cincinnati, OH

Corresponding author: Sona Kang, kangs@berkeley.edu

Received 12 July 2021 and accepted 12 October 2021

This article contains supplementary material online at https://doi.org/10.2337/figshare.16810945.

healthy subjects rapidly induces insulin resistance (23). Moreover, disrupting LPS-mediated signaling at the receptor level protects mice from developing inflammation and insulin resistance in response to chronic changes in dietary fat (24). As such, the elevation in LPS concentration/signaling could play a key role in low-grade systemic inflammation and insulin resistance in obesity; however, the underlying mechanisms are not fully understood.

It has been proposed that adipocytes themselves sense inflammatory signals and stimulate innate immune pathways. Indeed, adipocytes express immune receptors, including Toll-like receptors (TLRs; e.g., TLR2 and 4), that can sense inflammatory signals such as free fatty acids and LPS (24–26). By the same token, adipocytes express MHC proteins and are thus capable of acting as antigen-presenting cells to activate T cells (27). Furthermore, immune transcription factors, such as nuclear factor-κB (NF-κB) and interferon regulatory factor 3 (IRF3), have immune functions in adipocytes (28,29). However, we lack insight into how adipocytes use these immune proteins to mediate innate immune signals and how they associate with insulin resistance.

JMJD proteins are a class of proteins containing the Jumonji C (JmjC) domain, which is essential for their enzymatic activity, and 33 family members have been identified so far (30). Many of the JMJD proteins containing the canonical JmjC domain regulate various signaling and transcriptional pathways, thus affecting a diverse set of biological activities, including activities in adipose cells. For example, JMJD1A (31–33) and JMJD2B/KDM4B (34) promote adaptive thermogenesis by demethylating H3 lysine 9 (H3K9) di- or trimethylation, which are repressive histone marks. JMJD1C, also acting as a H3K9me2 demethylase, is required for adipogenesis and the full response to insulin-stimulated glucose uptake in 3T3-L1 adipocytes (35). In contrast, 10 of the JMJD members, including JMJD8, are characterized by their relatively small molecular weights (27–71 kDa) (36) and comprise a subfamily that is evolutionarily distant from the other conventional JMJD proteins (36). Little is known about their biological function to date. Our gene expression profiling studies identified that JMJD8 expression is highly enriched in adipocytes and is regulated by metabolic and nutritional states, implying its metabolic function in adipocytes.

In this study, we show that the expression of JMJD8 is affected by obesity, fasting, feeding, and insulin. In vitro studies demonstrate that JMJD8 was both necessary and sufficient to mediate insulin resistance in both mouse and human adipocytes. Congruently, whole-body *Jmjd8*-knockout (KO) mice displayed improved insulin sensitivity on an HFD and even on a chow diet. Conversely, adipocyte-specific *Jmjd8*-overexpressing mice exhibited aggravated insulin resistance and glucose intolerance on an HFD. In adipocytes, JMJD8 expression affected the gene program of several proinflammatory genes, which can trigger inflammation through cell-to-cell communication with macrophages. Lastly, we found that JMJD8 functionally interacted with IRF3, a proinflammatory factor that orchestrates adipocyte inflammation and insulin sensitivity. Together, these demonstrate that JMJD8 is a novel molecular nexus linking adipocyte insulin sensitivity and inflammation.

RESEARCH DESIGN AND METHODS

Cell Culture

3T3-L1 preadipocytes were obtained from American Type Culture Collection, and these cells were authenticated by the ability to differentiate and confirmed to be mycoplasma negative. To generate lentivirus particles, lentiviral constructs were cotransfected with pM2DG- and psPAX-expressing plasmids into 293T cells. After 48 h, virus-containing supernatant was collected, filtered through 0.45-mm filters, and added to mature 3T3-L1 adipocytes for 24 h along with 8 mg/mL polybrene. Transduction efficiency was determined by comparing to cells transduced in parallel with a GFP-expressing lentivirus. For the ex vivo system, subcutaneous adipose tissue from wild-type (WT) C57BL/6 mice was fractionated with digestion buffer (10 mg/mL collagenase D, 2.4 units of dispase II, and 10 mmol/L $CaCl_2$ in PBS). Simpson-Golabi-Behmel syndrome (SGBS) cells were maintained with DMEM/F12 and GlutaMAX. To differentiate SGBS cells, rosiglitazone (2 μmol/L), transferrin (0.01 mg/mL), cortisol (100 nmol/L), and triiodothyronine (0.2 nmol/L) were added in addition to isobutylmethylxanthine (250 μmol/L), insulin (20 nmol/L), and dexamethasone (25 nmol/L) from days 0–4.

Animals

Jmjd8-KO and Adi-Jmjd8-TG mice were generated at the Gene Targeting Facility at University of California Berkeley. Adipoq-Cre mice on the C57BL/6 background were obtained from The Jackson Laboratory (028020; Bar Harbor, ME). For chow and high-fat feeding studies, male C57BL/6J mice were put on the diet beginning at 9 weeks of age and continuing for 3 months. For histology, adipose tissues were fixed with neutral-buffered formalin and embedded in paraffin, and sections were stained with hematoxylin-eosin (H-E) at the Histology Core at Beth Israel Deaconess Medical Center. For the in vivo insulin signaling assay, after an overnight fast, insulin (10 units/kg for 10 min) or saline i.p. was given to WT and KO mice on HFD. After 10 min, various tissues were harvested and stored at –80°C until use. Tissue samples were homogenized in cell signaling lysis buffer containing protease inhibitors (Roche) and phosphatase inhibitors (Sigma-Aldrich) and subjected to Western blotting. All animal work was approved by the University of California Berkeley Animal Care and Use Committee.

Plasmids

Lentiviral overexpression vectors for JMJD8 and IRF3 were subcloned into pCDH at multicloning sites (*Mlu*I/*Nsi*I), and hairpins targeting *Jmjd8* were subcloned at *Age*I/*Eco*RI. Single guide RNAs (sgRNAs) targeting *Irf3* and human *JMJD8* were cloned into lentiCRISPR v2 vectors. Briefly, lentiCRISPRv2 plasmid was digested and dephosphorylated with *Bsm*BI. The sgRNA oligos were phosphorylated and annealed, followed by ligation into the digested lentiCRISPRv2 plasmid. Hairpin and sgRNA sequences are shown in Supplementary Table 2.

Reagents

2-Deoxy-D-[2,6-^{3}H]-glucose was purchased from Perkin-Elmer NEN Radiochemicals. Insulin, dexamethasone, isobutylmethylxanthine, rosiglitazone, thyroid hormone (triiodothyronine), glucose, 2-deoxyglucose (2-DG), and LPS came from Sigma-Aldrich. Mouse recombinant TNF-α was purchased from Millipore.

Antibodies

Antibodies were purchased from Cell Signaling Technology (9272, AKT; 3787, phosphorylated [p-]AKT [S473]; 2382, insulin receptor substrate 1 [IRS1]; 2118, GAPDH; 3033, p–NF-κB; 14269, histone H3; 4877, HSP90; 4302, IRF3; and 3025, insulin receptor [IR]), Santa Cruz Biotechnology (sc-515520, JMJD8; and sc-53566, Glut4), Sigma-Aldrich (F3165, Flag; and 4300653, phospho-IRS1 [S307]), Millipore (204359; NF-κB), Covance (MMS-101R, HA), GenScript (A01004; Ty1), and Invitrogen (44–816G, p-IRS1 [pY612]; and 44800G, p-IR [Y972]).

RNA Extraction and Quantitative PCR

Total RNA was extracted from tissues using TRIzol reagent according to the manufacturer's instructions. cDNA was reverse transcribed from 1 μg of RNA using the cDNA High-Capacity cDNA Reverse Transcription Kit (Applied Biosystems). Quantitative PCR (qPCR) was performed with SYBR Green qPCR Master Mix (AccuPower 2X; Bioneer Corporation) using a CFX96 Touch (Bio-Rad Laboratories) or QuantStudio 5 (Applied Biosystems). The relative amount of mRNA normalized to cyclophilin B was calculated using the delta–delta method. Primer sequences are listed in Supplementary Table 2.

Western Blotting

Cell or tissue culture samples were lysed in RIPA lysis buffer containing 50 mmol/L Tris-HCl (pH 7.5), 150 mmol/L NaCl, 1% Triton X-100, 0.1% SDS, and protease inhibitor cocktail for 30 min on ice with rotating samples. Protein concentration was quantified by Bradford or BSA analysis. Proteins were size fractionated by SDS-PAGE and then transferred to polyvinylidene difluoride or nitrocellulose membrane and detected using the ECL Assay Kit (cat. no. NEL104001EA; PerkinElmer). Immunoblots were quantified by ImageJ.

Nuclear Extraction

Cells or tissue were homogenized with hypotonic lysis buffer (10 mmol/L HEPES [pH 7.9], 1.5 mmol/L $MgCl_2$, 10 mmol/L KCl, 0.5 mmol/L dithiothreitol, and protease inhibitor cocktail) by 20 strokes of a loose-fitting pestle in a dounce homogenizer on ice. Supernatants were transferred into a new tube for cytosol-protein extraction after centrifugation at 2,000*g* for 10 min at 4°C, and the nuclear pellets were resuspended in 1 mL of hypotonic wash buffer and pelleted again by centrifugation at 2,000*g* for 1 min at 4°C. After the supernatants were removed, the washed nuclear pellets (retained as cleaner nuclei) were resuspended in 100 μL of RIPA lysis buffer and placed on ice for 30 min with occasional vortexing. The lysates were centrifuged at 15,000 rpm for 10 min at 4°C, and the supernatants were retained as high-purity nuclear proteins.

Chromatin Fractionation

Cells or tissue were homogenized with hypotonic lysis buffer (50 mmol/L HEPES [pH 7.5], 1.5 mmol/L $MgCl_2$, 10 mmol/L KCl, 1 mmol/L EDTA, 0.5 mmol/L dithiothreitol, and protease inhibitor cocktail) containing 0.04% Nonidet P-40 by 20 strokes of a loose-fitting pestle in dounce homogenizer on ice. Supernatants were transferred into a new tube for soluble cytosol-protein extraction after centrifugation at 2,000*g* for 10 min at 4°C, and the nuclear pellets were resuspended in 1 mL of hypotonic wash buffer and pelleted again by centrifugation at 2,000*g* for 1 min at 4°C. After the supernatants were removed, the washed nuclear pellets (retained as cleaner nuclei) were resuspended in 100 μL of RIPA lysis buffer and placed on ice for 40 min with occasional vortexing. The lysates were centrifuged at 15,000 rpm for 10 min at 4°C, and the supernatants were retained as chromatin fractionation.

Luciferase Assay

Analysis of LPS and TNF-α–stimulated luciferase activity, driven by a synthetic NF-κB or Ccl5 promoter, was conducted. Cells were cultured overnight in 24-well plates and transfected with a liposome complex containing pGL3/luciferase reporter gene (50 ng), Renilla (5 ng), and other relevant plasmids (400 ng). After 48 h, cells were treated with LPS (1 μg/mL) or TNF-α (10 ng/mL) for 6 h, washed with PBS, and solubilized with lysis buffer. The luciferase activity of cell extracts was determined using the dual-luciferase reporter assay system from Promega. To determine transfection efficiency, luciferase activity was normalized to Renilla activity.

Immunofluorescence Assay

Adipose tissues of *Jmjd8*-KO and Adi-Jmjd8-TG mice were fixed with neutral-buffered formalin and embedded in paraffin. Fixed tissues were permeabilized with PBS containing 0.1% Triton X-100 for 10 min and then incubated with anti-MAC2 antibodies in PBS containing

10% (v/v) FBS for 18 h at 4°C temperature. The coverslide was washed and incubated with FITC-conjugated anti-rat IgG for 1 h. Staining was analyzed with a confocal LSM710 microscope (Carl Zeiss Microimaging Inc.).

Coimmunoprecipitation

After washing cells with ice-cold PBS, cells were lysed with 1 mL lysis buffer, containing 50 mmol/L Tris-HCl (pH 7.5), 150 mmol/L NaCl, 1% Triton X-100, and protease inhibitor cocktail, for 30 min on ice with rotating samples. The lysates were centrifuged at 15,000 rpm for 10 min at 4°C, and then supernatants were incubated with anti-FLAG antibody-conjugated beads (Sigma-Aldrich) at 4°C for 2 h. The beads were washed four times with lysis buffer. Bound proteins were eluted by boiling in SDS sample buffer and separated by SDS-PAGE. Immunoblotting was performed following the standard procedures of a Western blot.

^{3}H-2-DG Assay

Various types of adipocytes were incubated in serum-free DMEM for 4–6 h. Cells were then washed three times with KRH buffer (12 mmol/L HEPES [pH 7.4], 121 mmol/L NaCl, 5 mmol/L KCl, 0.33 mmol/L $CaCl_2$, and 1.2 mmol/L $MgSO_4$) and incubated for 20 min in KRH buffer in the absence or presence of 100 nmol/L insulin. Cells were treated with 2-deoxy-D-[2,6–3H]-glucose (0.33 mCi/mL) for another 10 min. Glucose uptake was stopped quickly by three rapid washes with KRH buffer containing 200 mmol/L glucose and 10 mmol/L cytochalasin B on ice. Cells were solubilized in 0.1% SDS for 30 min, and radioactivity was measured by liquid scintillation counting.

Glucose Tolerance Test or Insulin Tolerance Test

For the insulin tolerance test (ITT), mice were fasted for 6 h and i.p. injected with insulin (0.5 units/kg for chow diet and 0.8 units/kg for HFD). Blood glucose was measured at 0, 15, 30, 60, 90, and 120 min. For the glucose tolerance test (GTT), mice were fasted for 6 h and i.p. injected with glucose (1.5 g/kg). Blood glucose levels were measured at 0, 15, 30, 60, and 120 min using the Contour Next glucometer and glucose strips.

Insulin ELISA

For the insulin ELISA, mice were fasted for 6 h. Plasma insulin was analyzed using an Ultrasensitive Mouse Insulin ELISA kit (cat. no. 90080; Crystal Chem). The end point calorimetric assays were performed using a Plate Reader SpectraMax i3. The IL-1β was analyzed using a mouse IL-1β uncoated ELISA kit (cat. no. 88-7013-22; Invitrogen). The end point calorimetric assays were performed using a Plate Reader SpectraMax i3.

Comprehensive Laboratory Animal Monitoring System Analysis

Metabolic rate was measured by indirect calorimetry in open-circuit Oxymax chambers, a component of the Comprehensive Laboratory Animal Monitoring System (CLAMS; Columbus Instruments). Mice were housed individually and maintained at 25°C under a 12-h light/12-h dark cycle. Activity was monitored in 1-min intervals of infrared beam breaks on the *x*-, *y*-, and *z*-axis and found not to be significantly different for any of the groups. Food and water were available ad libitum.

Coculture Studies

The adipocyte–macrophage coculture used the Transwell system (Corning, Corning, NY). 3T3-L1 adipocytes were cultured in six-well plates and differentiated at day 8, and macrophages (2×10^5 cells/well) were plated onto a Transwell insert containing a 0.4-μm polyethylene terephthalate membrane (Costar; Corning) in serum-free medium with or without the ligand (LPS). After incubating together for 24 h, the Transwell was removed, and 3T3-L1 adipocytes or macrophages were harvested for analysis.

RNA-Sequencing Library Generation and Analysis

RNA samples were extracted using the RNeasy Mini Kit (74104; Qiagen), and the quality of total RNA was assessed by the 2100 Bioanalyzer (Agilent Technologies) and agarose gel electrophoresis. Libraries were prepared using the BGI Library Preparation Kit, and sequencing was performed on the BGISEQ (Beijing Genomics Institute, Shenzhen, China). RNA-sequencing (RNA-seq) reads were aligned to the UCSC mm10 genome using STAR (37). rRNA and mitochondrial reads were removed. Differential expression analysis was done using edgeR (38), and differentially expressed genes upon KO were selected by fold change >1.5 and false discovery rate <0.05. Gene ontology analysis was performed using Enrichr (39). RNA-seq raw data are available in the Gene Expression Omnibus under accession number GSE164087.

Statistical Analysis

Data from three independent experiments, carried out in triplicate, were combined, and the results were presented as the mean ± SE. Statistical differences were assessed using Prism 4 (GraphPad Software). Unpaired two-tailed Student *t* tests and two-way ANOVA were used. A P value <0.05 was considered statistically significant.

Data and Resource Availability

Data sets generated from current study are available from the corresponding author.

RESULTS

JMJD8 Is Most Abundant in White Adipose Tissues and Has Increased Expression Under Hyperinsulinemic Conditions

Many members of the JMJD protein family are active in adipose tissue. Therefore, we characterized the expression of the small members of JMJD family to investigate

whether they are involved in the metabolic regulation of adipose tissue. Specifically, we characterized their expression in epididymal white adipose tissue (eWAT), a major visceral depot, from obesity-associated insulin-resistance models. Remarkably, *Jmjd8* was the only member with differential expression, increasing by three- and fivefold in diet-induced obesity and genetically obese *ob/ob* mouse models, respectively, compared with its expression in lean WT littermate controls (Fig. 1*A* and *B*). We confirmed that JMJD8 protein levels also increased in eWAT and inguinal WAT (iWAT) in both insulin-resistant models (Fig. 1*C–F*) to a similar degree as the transcript levels. Next, we studied whether adipose *Jmjd8* expression is regulated by nutritional state. Interestingly, 24 h of fasting resulted in a twofold reduction in *Jmjd8* mRNA expression in eWAT, and subsequent refeeding caused upregulation (Fig. 1*G*). Since insulin is a major hormone that increases after feeding, and obesity is strongly associated with hyperinsulinemia, we investigated whether insulin regulated *Jmjd8*. Indeed, insulin injection significantly increased adipose *Jmjd8* expression in C57BL/6 WT mice, especially when animals were challenged by an HFD (Fig. 1*H*). In addition, we asked whether inflammatory signals (i.e., TNF-α, LPS, and palmitate) increase JMJD8 levels, but none of them did (Supplementary Fig. 1*A* and *B*) Next, we studied the tissue distribution of JMJD8. Importantly, JMJD8 was expressed highest in adipose tissue, especially in white adipose depots, compared with other tissues, including liver and muscle (Fig. 1*I*). In addition to mature adipocytes, adipose tissue is comprised of multiple other cell types, including preadipocytes and macrophages, which are collectively termed the stromal vascular fraction (SVF). We thus compared *Jmjd8* levels between fractionated SVF versus the adipocyte fraction of eWAT and iWAT from lean C57BL/6 WT mice. We detected approximately five times higher enrichment in the adipocyte fraction compared with the SVF isolated from both depots (Fig. 1*J*). Congruent with this, *Jmjd8* expression was significantly induced at the differentiated stage of 3T3-L1, immortalized inguinal adipocytes, and brown adipocytes, compared with the preadipocyte stage of these models (Fig. 1*K–M*). Together, the enriched expression of JMJD8 in adipose tissue, especially in adipocytes, and the increased adipose expression under hyperinsulinemic conditions led us to hypothesize that JMJD8 regulates adipocyte metabolic function.

JMJD8 Inhibits Insulin Sensitivity in Adipocytes

Since JMJD8 levels increase during adipogenesis, we first examined whether JMJD8 regulates adipogenic potential by performing gain- and loss-of-function studies prior to differentiation. Knockdown of *Jmjd8* slightly reduced lipid accumulation, while overexpression of *Jmjd8* increased it, as assessed by Oil Red O staining (Supplementary Fig. 2*A* and *B*). *Jmjd8* knockdown adipocytes had reduced expression of *Pparg* and *Fabp4*, but not *Adipoq* and *Lep* (Supplementary Fig. 2*C*). In contrast, *Jmjd8* overexpressor adipocytes did not show marked changes in the expression of adipocyte markers (Supplementary Fig. 2*A–C*). Since Jmjd8 knockdown mildly affects adipogenesis, we sought to test the role of JMJD8 in the development of insulin resistance by knocking down *Jmjd8* expression in fully differentiated 3T3-L1 adipocytes at adipogenic day 8, achieving a 73% knockdown (Supplementary Fig. 3*A* and *B*), and no dedifferentiation was noted. Remarkably, *Jmjd8* knockdown increased insulin sensitivity by approximately twofold, as assessed by insulin-stimulated 2-deoxy-D-glucose uptake (Fig. 2*A*). Similar results were obtained when we knocked down *Jmjd8* in adipocytes differentiated from immortalized preadipocytes from the inguinal depot of lean WT mice (Fig. 2*B*). To see if the function of JMJD8 is conserved in humans, we used SGBS cells, a widely used human preadipocyte cell line that was derived from a human patient with SGBS (40), and knocked down JMJD8 using gRNA, thus achieving 50% knockdown efficiency (Supplementary Fig. 3*C*). Similar to mouse adipocytes, *JMJD8* knockdown significantly increased insulin-stimulated glucose uptake in SBGS adipocytes (Fig. 2*C*). Conversely, we conducted gain-of-function studies to determine if *Jmjd8* expression is sufficient to cause insulin resistance. We overexpressed JMJD8 in fully mature 3T3-L1 adipocytes, primary inguinal adipocytes, and human SGBS adipocytes (Supplementary Fig. 3*C–E*), which resulted in a 30–50% reduction in insulin-stimulated glucose uptake compared with control cells (Fig. 2*D–F*). Together, our results indicate that JMJD8 plays a causal role in the development of insulin resistance in mouse and human adipocytes in a cell-autonomous manner.

Jmjd8 KO Mice Are Protected From Diet-Induced Insulin Resistance and Glucose Intolerance

To confirm that JMJD8 plays a role in adipose and whole-body insulin sensitivity in vivo, we generated whole-body *Jmjd8* KO mice using the CRISPR/Cas9 system on the C57BL/6 background (Supplementary Fig. 4*A*). We validated complete *Jmjd8* KO by qPCR and Western blot in multiple tissues, including adipose (Fig. 3*A* and *B*). The KO mice were viable and showed normal growth compared with their WT littermate controls. On a chow diet, glucose tolerance was not different between genotypes (Fig. 3*C* and *D*), but KO mice exhibited increased insulin sensitivity (Fig. 3*E* and *F*). In addition, KO mice had a dramatic reduction in both fasting and fed insulin levels (Fig. 3*G*) and a lower HOMA of insulin resistance (HOMA-IR) (Fig. 3*H*). This was without alterations in body weight (Supplementary Fig. 4*B*) or body composition, as assessed by EchoMRI and tissue weight (Supplementary Fig. 4*C* and *D*). Together, these data suggest that *Jmjd8*-KO mice have increased whole-body insulin

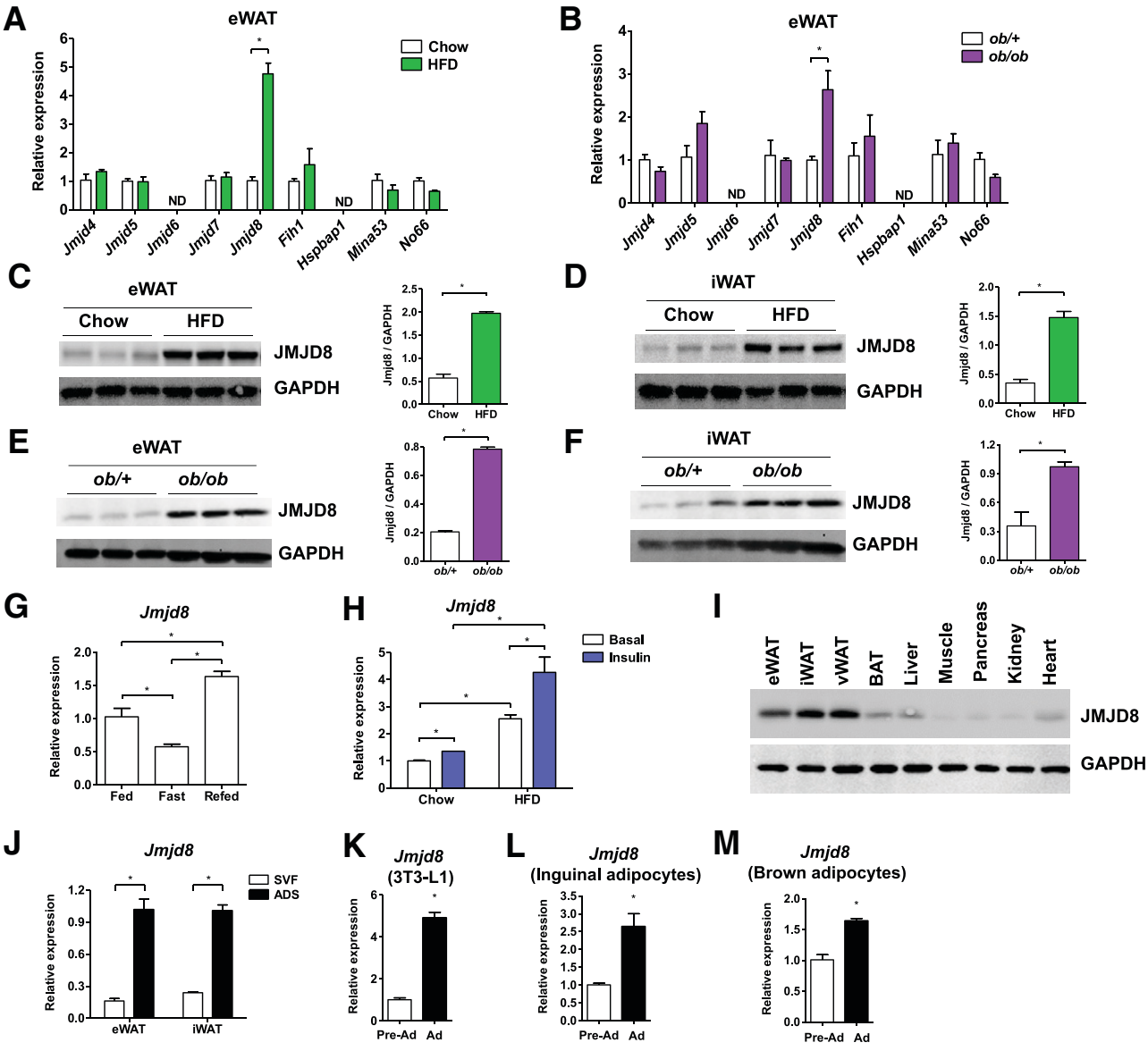

Figure 1—JMJD8 is abundant in WATs, enriched in adipocytes, and increases under hyperinsulinemic conditions. The mRNA level of various small JMJD proteins in eWAT from C57BL/6 WT mice on chow vs. HFD mice (*A*) and *ob*/+ vs. *ob*/*ob* mice (*B*) ($n = 3$ mice; $^*P < 0.05$, two-way ANOVA with Student *t* test, mean ± SEM). JMJD8 protein levels in eWAT and iWAT from C57BL/6 WT mice on chow vs. HFD (*C* and *D*) or *ob*/+ vs. *ob*/*ob* mice (*E* and *F*, left panels). JMJD8 protein levels with quantification by normalizing with GAPDH ($n = 3$ mice; $^*P < 0.05$, Student *t* test, mean ± SEM) (*E* and *F*, right panels). *G*: *Jmjd8* mRNA levels in eWAT from C57BL/6 mice at fed, fasting (24 h), and refed (24 h) states ($n = 5$ mice; $^*P < 0.05$, one-way ANOVA with Student *t* test, mean ± SEM). *H*: *Jmjd8* mRNA level was measured in eWAT from C57BL/6 WT mice on chow vs. HFD with i.p. injection of insulin (10 U/kg, 3 h) or vehicle after 16-h fasting ($n = 3$ mice; $^*P <$ 0.05, two-way ANOVA with Student *t* test, mean ± SEM). *I*: JMJD8 protein expression in various tissues from WT C57BL/6 mice on chow. *J*: *Jmjd8* mRNA level in mature adipocytes (ADS) vs. the SVF ($n = 4$ mice; $^*P < 0.05$, two-way ANOVA with Student *t* test, mean ± SEM). *K* and *M*: *Jmjd8* mRNA levels in 3T3-L1, iWAT, and brown adipose tissue at confluent preadipocyte (Pre-Ad) vs. mature adipocyte (Ad) stages ($n = 3$; $^*P < 0.05$, one-way ANOVA with Student *t* test, mean ± SEM). BAT, brown adipose tissue; vWAT, visceral WAT.

sensitivity on a chow diet without changes in energy homeostasis.

Since we found increased JMJD8 expression in response to high-fat feeding, we tested whether *Jmjd8* deficiency confers protection from diet-induced insulin resistance. For that, a cohort of mice were placed on an HFD (58% calories from fat), and we found a trend toward KO mice gaining less weight, but the difference did not reach statistical significance (Fig. 4*A*). Consistent with this, EchoMRI studies indicated that there were no marked differences in body composition (Fig. 4*B*) or the mass of various adipose tissues, including eWAT, iWAT,

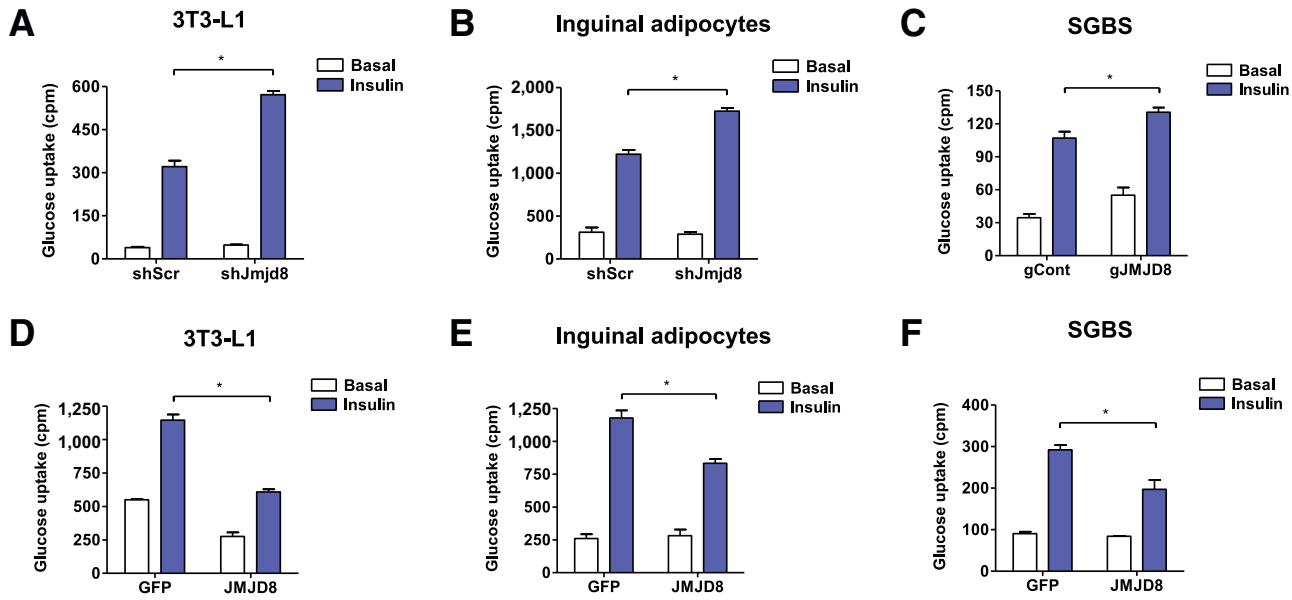

Figure 2—JMJD8 is both necessary and sufficient to mediate insulin resistance in mouse and human adipocytes. Basal and insulin-stimulated glucose uptake measured by a ^{3}H-2-DG assay in mature 3T3-L1 adipocytes (*A*), primary inguinal adipocytes (*B*), or human SGBS adipocytes (*C*) that were infected with control shScramble (shScr) vs. hairpin against *Jmjd8* (shJmjd8) or control gRNA (gCont) vs. gRNA against *JMJD8* (gJMJD8) (n = 4; *P < 0.05, two-way ANOVA with Student t test, mean ± SEM). Basal and insulin-stimulated glucose uptake measured by a ^{3}H-2-DG assay in mature 3T3-L1 adipocytes (*D*), primary inguinal adipocytes (*E*), or human SGBS adipocytes (*F*) that were infected with lentivirus expressing GFP vs. JMJD8 (n = 4; *P < 0.05, two-way ANOVA with Student t test, mean ± SEM).

and mesenteric WAT (Fig. 4*C*). To further assess energy homeostasis, the indirect calorimetry of a cohort of high-fat–fed mice was analyzed using CLAMS. We confirmed that KO mice did not display a significant change in their energy balance, locomotor activity, or food intake (Supplementary Fig. 5). Despite no major changes in energy homeostasis, remarkably, *Jmjd8*-KO mice on an HFD exhibited a significant improvement in glucose tolerance (Fig. 4*D* and *E*) and insulin sensitivity compared with controls (Fig. 4*F* and *G*). Similar to the chow-fed cohort, KO mice had a dramatic reduction in serum insulin levels in both fed and fasting conditions and improved HOMA-IR compared with WT mice (Figs. 4*H* and *I*).

To better assess insulin responsiveness in various metabolic tissues, we performed in vivo insulin signaling assays on tissues from WT and *Jmjd8*-KO mice on an HFD. After fasting overnight, animals received a dose of bolus insulin (10 U/kg, 10 min) via i.p. injection, and then the tissues were collected and subjected to immunoblotting analysis for the phosphorylated and total protein fractions of insulin signaling components. We noted that phosphorylation levels associated with the active forms of IRS1, IR, and AKT were increased in the KO eWAT when normalized to total protein levels (Fig. 4*J*, *K*, *N*, and *O*). Interestingly, KO eWAT showed reduced phosphorylation of IRS1 at serine 307 (Fig. 4*J* and *L*), which was shown to be implicated in the counterregulatory feedback of insulin signaling by enhancing IRS1 protein degradation (41–43). We indeed noted a trend toward increased protein expression of IRS1 in the KO eWAT (Fig. 4*M*). By contrast, we did not observe significant changes in the active phosphorylation of AKT in other metabolic tissues (Supplementary Fig. 6*A*–*F*). Moreover, pyruvate tolerance was indistinguishable between genotypes, suggesting that there was no hepatic contribution to the improved glucose homeostasis of KO mice (Supplementary Fig. 6*G*). To verify improved insulin sensitivity in KO adipocytes, we conducted ex vivo insulin-stimulated glucose uptake assays on WT versus KO mouse adipocytes fractioned using collagenase digestion and found that KO adipocytes exhibit an approximately twofold increase in insulin-stimulated glucose uptake (Fig. 4*P*). Lastly, we measured the mRNA and protein expression of insulin-dependent glucose transporter GLUT4 (*Slc2a4*) and noted, overall, increased expression in the KO eWAT (Fig. 4*Q*–*S*), which is likely to contribute to the improved insulin sensitivity. Together, our results suggest that *Jmjd8* deficiency leads to improved adipose and systemic insulin sensitivity by involving improved insulin signal transduction and increased GLUT4 expression in adipose tissue.

Adipose-Specific *Jmjd8* Overexpression Exacerbates Diet-Induced Glucose Intolerance and Insulin Resistance

Next, we performed JMJD8 gain-of-function studies in vivo. We generated *Jmjd8* transgenic mice on a C57BL/6

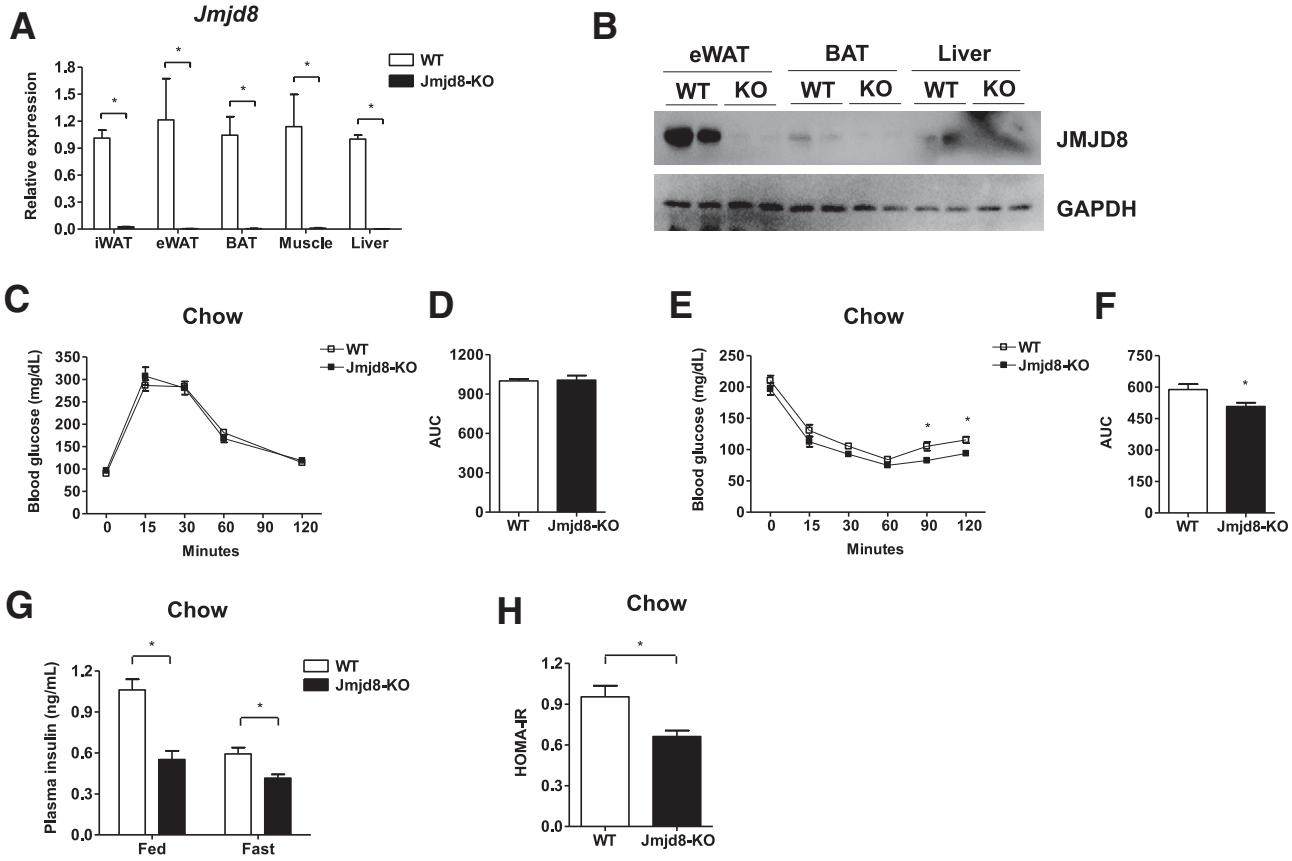

Figure 3—*Jmjd8*-KO mice exhibit increased insulin sensitivity on chow. Knockdown efficiency of *Jmjd8* mRNA (*A*) and protein (*B*) in various tissues from WT vs. *Jmjd8*-KO mice ($n = 3$ mice; $^*P < 0.05$, two-way ANOVA with Student *t* test, mean ± SEM). *C* and *D*: GTT on WT vs. *Jmjd8*-KO mice on chow ($n = 8$ mice; $^*P < 0.05$, two-way ANOVA with Student *t* test, mean ± SEM). *E* and *F*: ITT on WT vs. *Jmjd8*-KO mice on chow ($n = 8$ mice; $^*P < 0.05$, two-way ANOVA with Student *t* test, mean ± SEM). *G*: Fed and fasting insulin levels for WT and *Jmjd8*-KO mice on chow ($n = 5$ mice; $^*P < 0.05$, two-way ANOVA with Student *t* test, mean ± SEM). *H*: HOMA-IR for WT vs. *Jmjd8*-KO mice on chow ($n = 5$ mice; $^*P < 0.05$, Student *t* test, mean ± SEM). AUC, area under the curve; BAT, brown adipose tissue.

background, in which *Jmjd8* transgene expression was induced in a Cre-dependent manner (tagged by the Ty1 tag) (Supplementary Fig. 7). These mice were crossed to adiponectin Cre (44) mice (Supplementary Fig. 7) to generate adipocyte-specific overexpressor mice (Adi-Jmjd8-TG). As a result, we achieved a physiological level of overexpression (two- to fivefold) in iWAT, eWAT, and brown adipose tissue but not in other tissues (Fig. 5*A* and *B*). Adi-Jmjd8-TG mice were viable and showed normal growth compared with their littermate controls. On a chow diet, there were no marked differences in body weight, body composition, or tissue mass between genotypes, and no obvious differences were detected between genotypes using a GTT or ITT (not shown). On an HFD, there were no significant changes in body weight or body composition compared with controls (Fig. 5*C–E*) and no marked difference in energy homeostasis, assessed by CLAMS analysis, between genotypes (Supplementary Fig. 8). Without major advantages in body weight or adiposity, Adi-Jmjd8-TG mice on an HFD exhibited worsened glucose tolerance and insulin sensitivity (Fig. 5*F–I*), accompanied by higher insulin levels and higher HOMA-IR compared with control WT mice on an HFD (Fig. 5*J* and *K*). In addition, we measured the mRNA and protein expression of GLUT4 and found its expression level was decreased in the Adi-Jmjd8-TG eWAT (Fig. 5*L–N*). Consistent with in vivo results, we noted that *Jmjd8* overexpression in 3T3-L1 adipocytes overall show reduced insulin signal transduction in adipocytes (Fig. 5*O–T*). Together, these results suggest that adipocyte-specific JMJD8 overexpression exacerbates systemic insulin resistance when challenged by HFD.

Jmjd8 Deficiency Improves Adipose Tissue Inflammation in an Adipocyte-Autonomous Manner

To understand the downstream molecular mechanisms by which JMJD8 mediates adipose insulin resistance, we profiled the adipose tissue transcriptome of WT and KO mice fed an HFD for 2 months. We identified 151 and 302 genes that were up- and downregulated in the KO tissues, respectively (Fig. 6*A* and Supplementary Table 1). To determine if specific biological processes and functions were affected by *Jmjd8* deficiency, gene ontology analysis

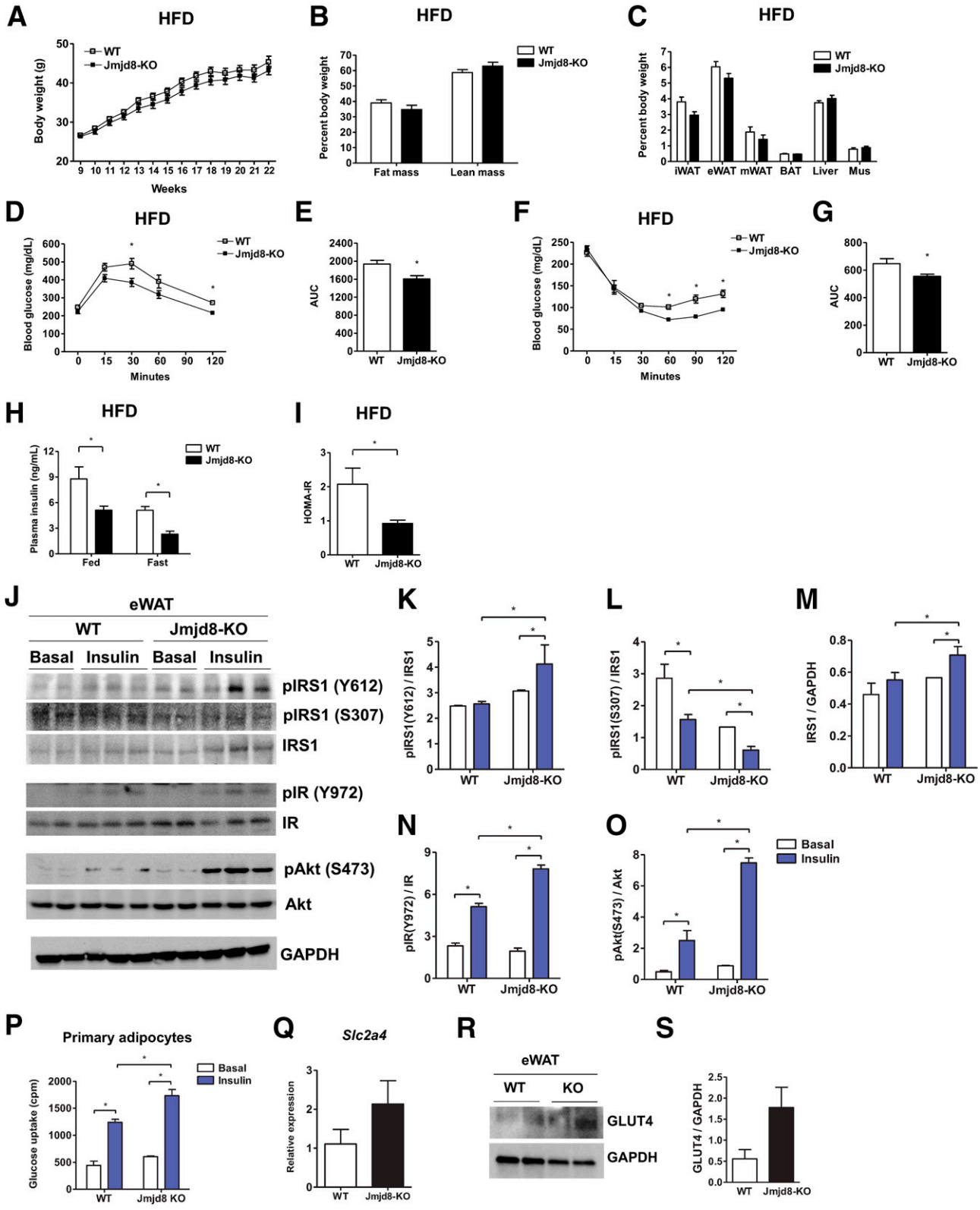

Figure 4—*Jmjd8*-KO mice exhibit improved insulin sensitivity and glucose tolerance on HFD. *A*: Body weight of WT and *Jmjd8*-KO mice on HFD (n = 18 mice; $P < 0.05$, two-way ANOVA with Student t test, mean ± SEM). *B*: Body composition after 11 weeks of HFD (n = 8 mice; $P < 0.05$, two-way ANOVA with Student t test, mean ± SEM). *C*: Tissue weight per body weight after 11 weeks of HFD (n = 6 mice; $P < 0.05$, two-way ANOVA with Student t test, mean ± SEM). *D* and *E*: GTT for WT and *Jmjd8*-KO mice on HFD (n = 6 mice; *$P < 0.05$, two-way ANOVA with Student t test, mean ± SEM). *F* and *G*: ITT for WT and *Jmjd8*-KO mice on HFD (n = 6 mice; *$P < 0.05$, two-way ANOVA with Student t test, mean ± SEM). *H*: Fed and fasting insulin levels for WT and *Jmjd8*-KO mice on HFD (n = 6 mice; *$P < 0.05$,

was performed. While no gene ontology terms were found to be significantly enriched in upregulated genes (not shown), inflammation and chemotaxis pathways were enriched in downregulated genes (Fig. 6*B*). Also, we confirmed reduced expression of several top-regulated genes and additional genes involved in inflammation, including *Il1b*, *Ccl2*, *Il6*, *Tnf*, and *Lcn2*, in the KO eWAT (Fig. 6*C*). Conversely, those inflammatory genes were coordinately upregulated in obese *Jmjd8* transgenic eWAT compared with control tissue (Fig. 6*D*). A reduced serum level of IL-1b was also confirmed by ELISA in obese KO mice compared with WT mice (Fig. 6*E*). Histological studies found that macrophage infiltration was reduced in obese *Jmjd8* KO eWAT compared to obese control tissue, as indicated by reductions in the numbers of crownlike structures and fewer cells stained with a macrophage marker (Mac-2), as detected by H-E and immunofluorescence staining (Fig. 6*F* and *H*). Conversely, macrophage infiltration was increased in obese *Jmjd8*-TG eWAT compared with obese control tissue (Fig. 6*G* and *I*). We also saw a concordant change in the expression of *Cd11b*, one of the surface markers for macrophages (Supplementary Fig. 9*A*). Macrophage polarity often shifts in obesity from alternative M2 to classical M1, thus promoting proinflammatory signaling via secreting proinflammatory cytokines. Obese *Jmjd8*-KO eWAT had increased expression of M2 markers (i.e., *Tgfb1*, *ll10*, *Arg1*, and *Mgl2*) (Supplementary Fig. 9*A*) in parallel with reduced expression of M1 markers (i.e., *Il1b*, *Tnf*, *Ccl2*, and *Il6*) compared with controls, implying that there might be a macrophage polarization toward M2. Although obese *Jmjd8*-TG eWAT had increased expression of M1 markers, there were no major differences in the expression of M2 markers (Supplementary Fig. 9*B*).

Since we used whole fat tissue for gene profiling and that the gene deletion occurs in all cells, we cannot exclude the possibility that some of the transcriptional changes came from immune cells such as macrophages. To dissect out the specific role of JMJD8 in inflammation in adipocytes versus macrophages, we conducted the following experiments. In order to determine the adipocyte autonomous role of JMJD8 in the regulation of inflammation, we measured a subset of inflammatory genes after altering JMJD8 levels in 3T3-L1 adipocytes. *Jmjd8* knockdown suppressed the mRNA expression of several inflammatory genes (Fig. 6*J*), whereas *Jmjd8* overexpression increased them (Fig. 6*K*). Next, we investigated if there is cross talk between these two cell types by conducting coculture experiments. First, we cocultured WT RAW264.7 macrophages in the upper chamber of the Transwell system and 3T3-L1 adipocytes with altered *Jmjd8* expression in the lower chamber (Supplementary Fig. 10*A*). Importantly, WT macrophages cocultured with conditioned media from the JMJD8-overexpressing 3T3-L1 adipocytes had increased expression of inflammatory genes and reduced expression with *Jmjd8* silenced adipocytes (Supplementary Fig. 10*B* and *C*). We also conducted the converse experiment by coculturing WT 3T3-L1 adipocytes with bone marrow–derived *Jmjd8* KO and WT macrophages (Supplementary Fig. 10*D*). In this case, there were no discernable changes in the expression of inflammatory genes in adipocytes (Supplementary Fig. 10*E*) and no discernable change in insulin-stimulated glucose uptake (Supplementary Fig. 10*F*). Together, these results suggest that JMJD8's regulatory role in inflammation and insulin resistance primarily stems from adipocytes, not macrophages.

JMJD8 Is Required for LPS-Mediated Inflammatory Gene Induction Through Functional Interaction With IRF3

Given JMJD8's effect on inflammatory genes and insulin resistance, we tested whether *Jmjd8* knockdown prevents insulin resistance mediated by inflammatory signals. *Jmjd8* was knocked down in mature 3T3-L1 adipocytes using hairpins against *Jmjd8* or control and treated with LPS or vehicle plus ATP. Interestingly, *Jmjd8*-knockdown adipocytes were selectively protected from the effects of LPS/ATP (Fig. 7*A*). An analogous experiment was performed using human SGBS adipocytes, and similar results were found (Fig. 7*B*). In line with these results, *Jmjd8* KO mouse and human adipocytes showed attenuated LPS-mediated inflammatory gene stimulation, whereas JMJD8 overexpression enhanced the response (Fig. 7*C* and *D*). By contrast, *Jmjd8* knockdown did not have a discernable effect on either TNF-α–mediated insulin resistance or its inflammatory gene stimulation (Supplementary Fig. 11). Together, our data indicate that JMJD8 is necessary in LPS-mediated, but not TNF-α–mediated, inflammation and insulin-stimulated glucose uptake.

Given that JMJD8 is necessary for LPS-mediated insulin resistance, we investigated whether JMJD8 alters downstream signaling pathways upon LPS stimulation. Adipocytes recognize LPS through TLR4 and subsequently initiate two arms of inflammatory pathways that depend on the MyD88 and TRIF signaling pathways (45). MyD88-dependent signaling activates NF-κB–dependent events, whereas TLR4/TRIF-dependent signaling results in TANK-binding kinase 1 (TBK1) and IκB kinase ε (IKKε) activation and triggers IRF3-dependent responses (45). Importantly,

two-way ANOVA with Student *t* test, mean ± SEM). *I*: HOMA-IR on WT and *Jmjd8*-KO mice on HFD ($n = 6$ mice; $^*P < 0.05$, Student *t* test, mean ± SEM). *J*: Insulin signaling assays on *Jmjd8*-KO mice on HFD. Immunoblot of total and p-IRS1, -IR, and -Akt in eWAT was performed on WT and *Jmjd8*-KO mice after i.p. injection of insulin (10 units/kg, 10 min) ($n = 2$ and 3 mice). *K–O*: Quantification of Western blot in *J* ($^*P < 0.05$, two-way ANOVA with Student *t* test, mean ± SEM). *P*: Basal and insulin-stimulated glucose uptake (^{3}H-2-DG assay) using primary inguinal adipocytes from WT and *Jmjd8*-KO mice ($n = 6$; $^*P < 0.05$, two-way ANOVA with Student *t* test, mean ± SEM). *Q–S*: GLUT4 (*Slc2a4*) mRNA and protein expression in obese WT and *Jmjd8*KO eWAT. AUC, area under the curve.

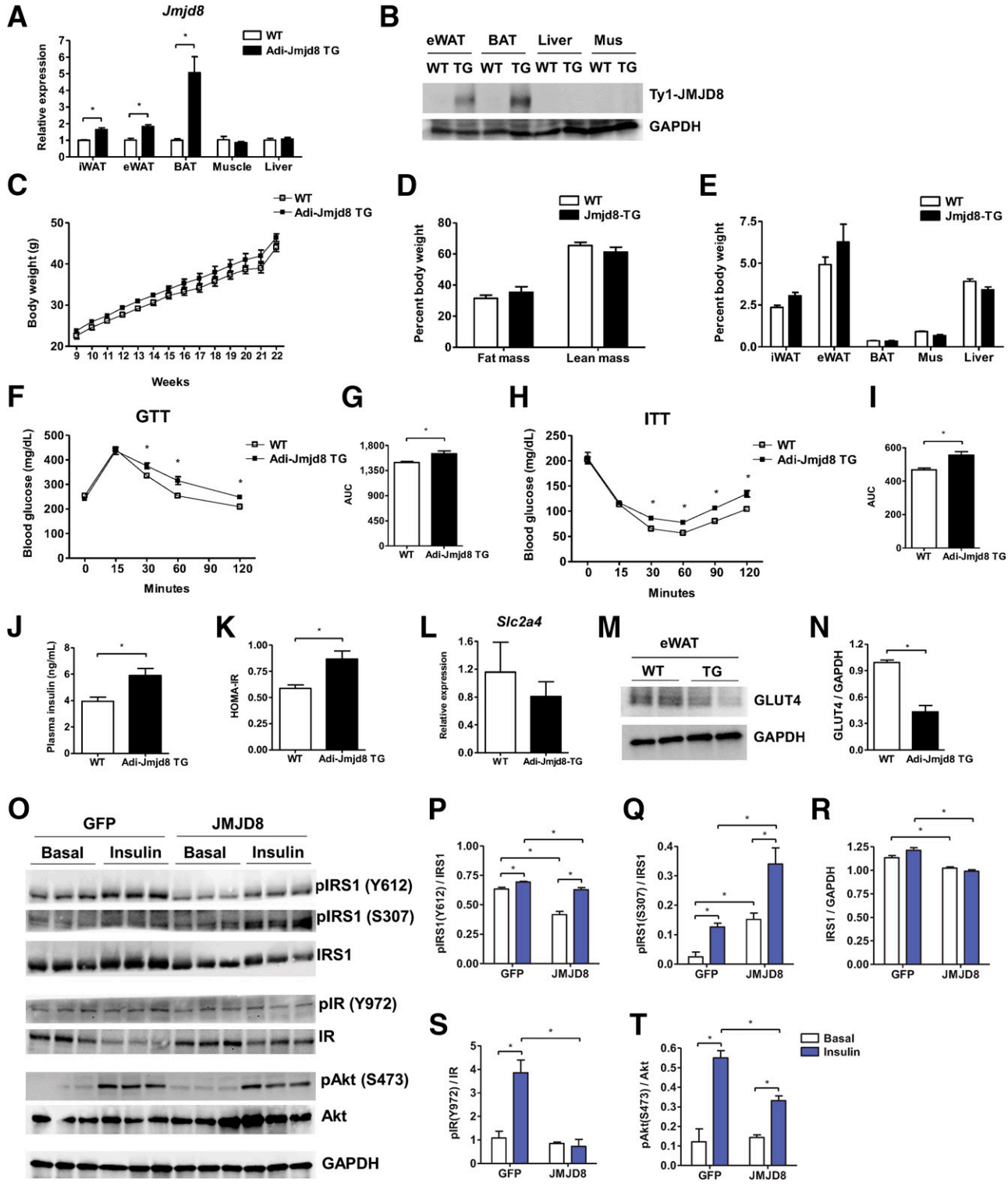

Figure 5—Adi-Jmjd8-TG mice are more susceptible to diet-induced insulin resistance and glucose intolerance. Expression levels of *Jmjd8* mRNA (*A*) and protein (*B*) in various tissues from WT vs. Adi-Jmjd8-TG mice. The overexpression was confirmed by detecting JMJD8 tagged with a Ty1 epitope in the transgene ($n = 2$ mice; $^*P < 0.05$, Student *t* test, mean ± SEM). *C*: Body weight of WT and Adi-Jmjd8-TG mice on HFD ($n = 6$ mice; $P < 0.05$, two-way ANOVA with Student *t* test, mean ± SEM). *D*: Body composition of WT and Adi-Jmjd8-TG mice on HFD ($n = 7$ and 5 mice; $P < 0.05$, two-way ANOVA with Student *t* test, mean ± SEM). *E*: Tissue weight per body weight of WT and Adi-Jmjd8-TG mice on HFD ($n = 3$ mice; $P < 0.05$, two-way ANOVA with Student *t* test, mean ± SEM). *F* and *G*: GTT of WT and Adi-Jmjd8-TG mice on HFD ($n = 6$ mice; $^*P < 0.05$, two-way ANOVA with Student *t* test, mean ± SEM). *H* and *I*: ITT for WT and Adi-Jmjd8-TG mice on HFD ($n = 7$ and 6 mice; $^*P < 0.05$, two-way ANOVA with Student *t* test, mean ± SEM). *J*: Fasting insulin levels for WT and Adi-Jmjd8-TG mice on HFD ($n = 7$ and 6 mice; $^*P < 0.05$, Student *t* test, mean ± SEM). *K*: HOMA-IR of WT and Adi-Jmjd8-TG mice on HFD

these two transcription factors activate distinct but overlapping sets of target genes and, in some cases, may cooperate functionally and physically to activate inflammatory genes (46,47). We did not detect any marked changes in the canonical regulation of NF-κB caused by JMJD8 alterations, as evidenced by the lack of clear changes in nuclear localization in both obese *Jmjd8*-KO and -TG eWAT compared with control tissues (Supplementary Fig. 12*A*). We did not detect changes in the levels of total or Ser536 phosphorylated NF-κB during *Jmjd8* knockdown or overexpression in the presence or absence of LPS stimulation (Supplementary Fig. 12*B*–*G*), and there was no physical interaction between JMJD8 and the upstream regulators of NF-κB signaling, such as IκB or IKKβ (Supplementary Fig. 12*H* and *I*). Lastly, JMJD8 did not alter TNF-α– or LPS-driven transcriptional activity when assessed by NF-κB reporter assays (Supplementary Fig. 12*J* and *K*).

Next, we sought to determine whether JMJD8 is involved in IRF3-mediated signaling. Remarkably, we found that JMJD8 coimmunoprecipitated with IRF3 (Fig. 8*A*), and thus, we performed epistasis experiments to dissect the functional interaction between JMJD8 and IRF3. First, we determined whether JMJD8 requires IRF3 to mediate its actions by introducing *Irf3* gRNA and/or WT *Jmjd8* into mature L1 adipocytes. Strikingly, we found that JMJD8 was no longer able to inhibit insulin-stimulated glucose uptake without IRF3 (Fig. 8*B*). In line with this, JMJD8's ability to enhance LPS-stimulated induction of inflammatory genes, especially *Tnf* and *Il6*, was completely abolished by losing IRF3 (Fig. 8*C*–*E*). Next, we asked whether IRF3 requires JMJD8 to promote inflammation and insulin resistance in the presence and absence of LPS by introducing the expression vectors for *Jmjd8* hairpins and WT *Irf3* in mature L1 adipocytes. We found that IRF3's ability to inhibit insulin-stimulated glucose uptake or IRF3's ability to induce inflammatory genes was marginally affected by losing JMJD8 (Supplementary Fig. 13*A*–*D*). Altered JMJD8 expression also did not affect the chromatin localization of IRF3 (Supplementary Fig. 13*E*) or the IRF3-driven transcriptional activity when assessed by IRF3 reporter assay (Supplementary Fig. 13*F*). Together, our data suggest JMJD8 requires IRF3 to mediate insulin resistance and inflammation in adipocytes and not the reverse.

We propose a model in which chronic overnutrition increases the adipocyte level of JMJD8, which then interacts with IRF3 to activate proinflammatory genes, thus causing the recruitment of proinflammatory immune cells and adipocyte insulin resistance.

DISCUSSION

Adipose tissue inflammation, characterized by immune cell infiltration and cytokine secretion, has been implicated as a major player in both the onset of metabolic syndrome and the associated pathophysiological consequences, including insulin resistance (1,48). During these processes, a dynamic interplay operates between adipocytes and immune cells. Although it has been suggested that adipocytes themselves play an important role in sensing and triggering inflammation and attracting immune cells (24,26,27,29), there is a paucity of studies that elucidate the molecular machinery that mediates inflammation during overnutrition. In this study, we demonstrate that JMJD8 acts as a molecular nexus that mediates adipocyte inflammation and insulin sensitivity.

We found that JMJD8 expression was highly enriched in adipose tissue, especially in the adipocyte fraction, relative to other tissues. The expression pattern of adipose JMJD8 in insulin resistance models and its dynamic regulation in response to nutritional states and insulin levels led us to explore the metabolic function of JMJD8 in adipose insulin sensitivity. We demonstrated that JMJD8 was both necessary and sufficient to mediate insulin resistance in both mouse and human adipocytes. Moreover, we proved the in vivo role of adipose JMJD8 using KO and transgenic mouse models. Our RNA-seq studies revealed that insulin resistance in *Jmjd8*-KO mice was accompanied by reduced inflammation. We then showed that JMJD8 gain- and loss-of-function coordinately regulated the transcriptional program of several inflammatory genes in adipocytes. Furthermore, we demonstrated that JMJD8 played a necessary role in LPS-stimulated inflammation and insulin resistance through a functional interaction with IRF3.

JMJD8 is a small-molecular-weight JMJD protein (36). While some JMJD proteins with large molecular weights possess histone demethylase activity, it does not seem to be the case with JMJD8. Its JmjC domain has a noncanonical $HXHX_nH$ motif compared with other JmjC proteins with $HX(D/E)X_nH$ (30). Moreover, JMJD8 does not contain any other functional domain, such as C2H2/C5H2 or AT-hook motifs, that are implicated in binding or interacting with DNA (49). By contrast, a recent study proposed that JMJD8 may act as a transcriptional repressor, as ectopic expression of an N-terminal truncation mutant localizes to gene promoters and represses them (50). However, so far, there is no report describing the existence of an endogenous form of JMJD8 with an N-terminal truncation, raising doubts about such JMJD8 nuclear activity. In support of this, our localization analysis found JMJD8 mainly in the cytosol under basal conditions and after stimulation by TNF-α and LPS (not shown). Therefore, we postulate that the repressive role for JMJD8 in the transcriptional program of proinflammatory cytokines is indirect and is

(n = 7 and 6 mice; *$P < 0.05$, Student t test, mean ± SEM). *L*–*N*: GLUT4 (*Slc2a4*) mRNA and protein in obese WT and Adi-Jmjd8-TG eWAT. *O*–*T*: Insulin signaling assays on 3T3L1 adipocytes overexpress JMJD8 and GFP (n = 3; *$P < 0.05$, two-way ANOVA with Student t test, mean ± SEM). BAT, brown adipose tissue; Mus, muscle.

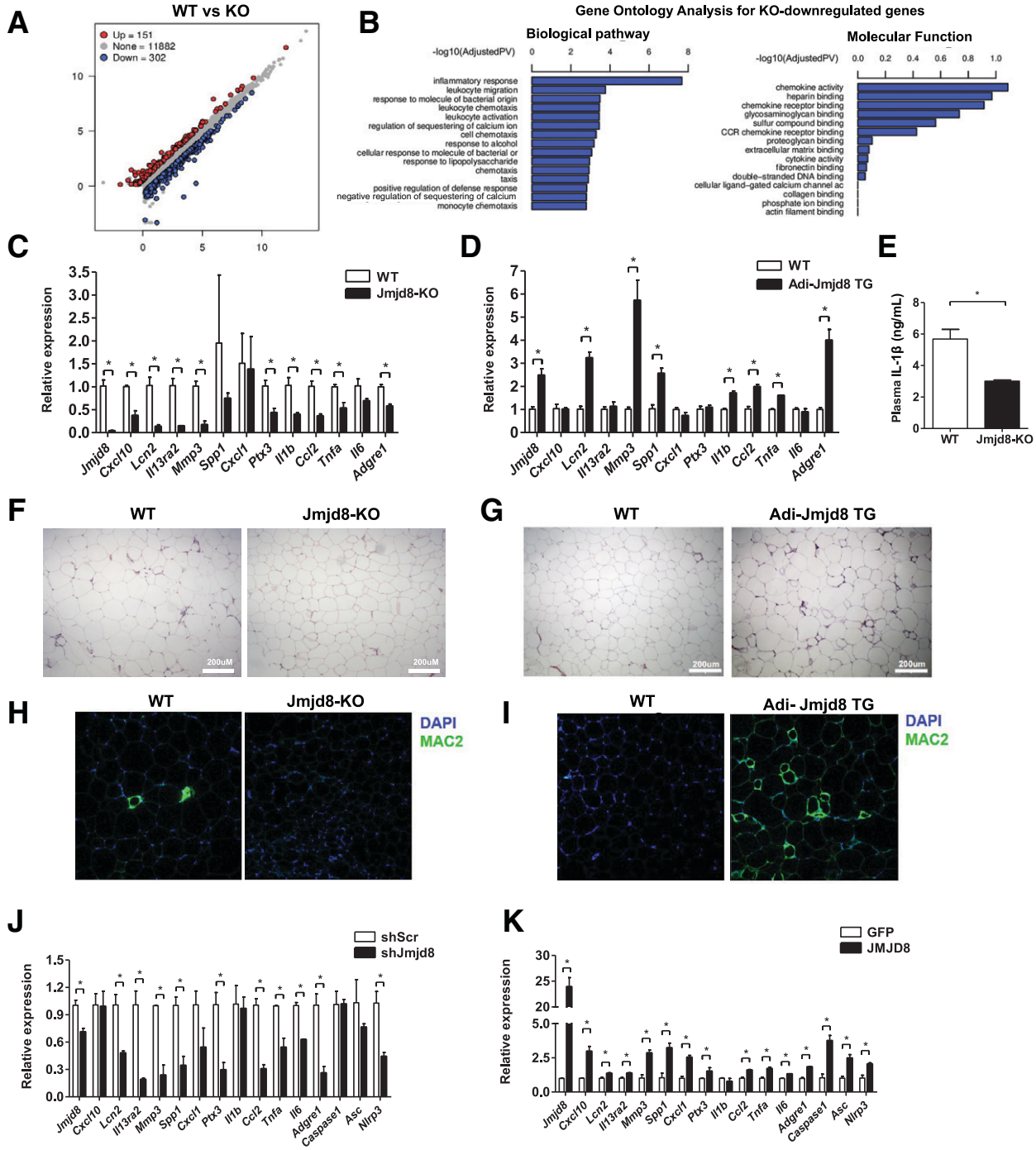

Figure 6—JMJD8 regulates inflammatory genes in adipose tissue. *A*: RNA-seq of eWAT from WT vs. *Jmjd8*-KO mice on HFD. The scatterplot shows differentially regulated genes in *Jmjd8*KO eWAT (n = 3 mice; fold change >1.5 and false discovery rate <0.05). *B*: Biological pathways analysis from up- and downregulated genes in *Jmjd8*-KO samples. *C*: qPCR validation of upregulated genes in eWAT from WT and *Jmjd8*-KO mice on HFD (n = 3 mice; *$P < 0.05$, Student t test, mean ± SEM). *D*: qPCR analysis of upregulated genes in eWAT from WT and Adi-Jmjd8-TG mice on HFD (n = 3 mice; *$P < 0.05$, Student t test, mean ± SEM). *E*: Serum IL-1β levels for WT and *Jmjd8*-KO mice on HFD (n = 8 mice; *$P < 0.05$, Student t test, mean ± SEM). H-E staining and Mac2 staining of obese eWAT from WT vs. *Jmjd8*-KO mice (*F* and *H*) or WT vs. Adi-Jmjd8-TG mice (*G* and *I*). qPCR analysis of the JMJD8 target genes in 3T3-L1 adipocytes infected with hairpin against *Jmjd8* (shJmjd8) vs. hairpin (*J*) or GFP vs. *Jmjd8* (*K*) (n = 3; *$P < 0.05$, Student t test, mean ± SEM). shScr, shScramble.

likely via interfering with a signaling cascade in the cytosol. A recent proteomics study reported that JMJD8 contains N-terminal sequence that enables it to localize to the luminal endoplasmic reticulum (ER) (51), where it can interact with ER proteins involved in protein folding and complex formation. However,

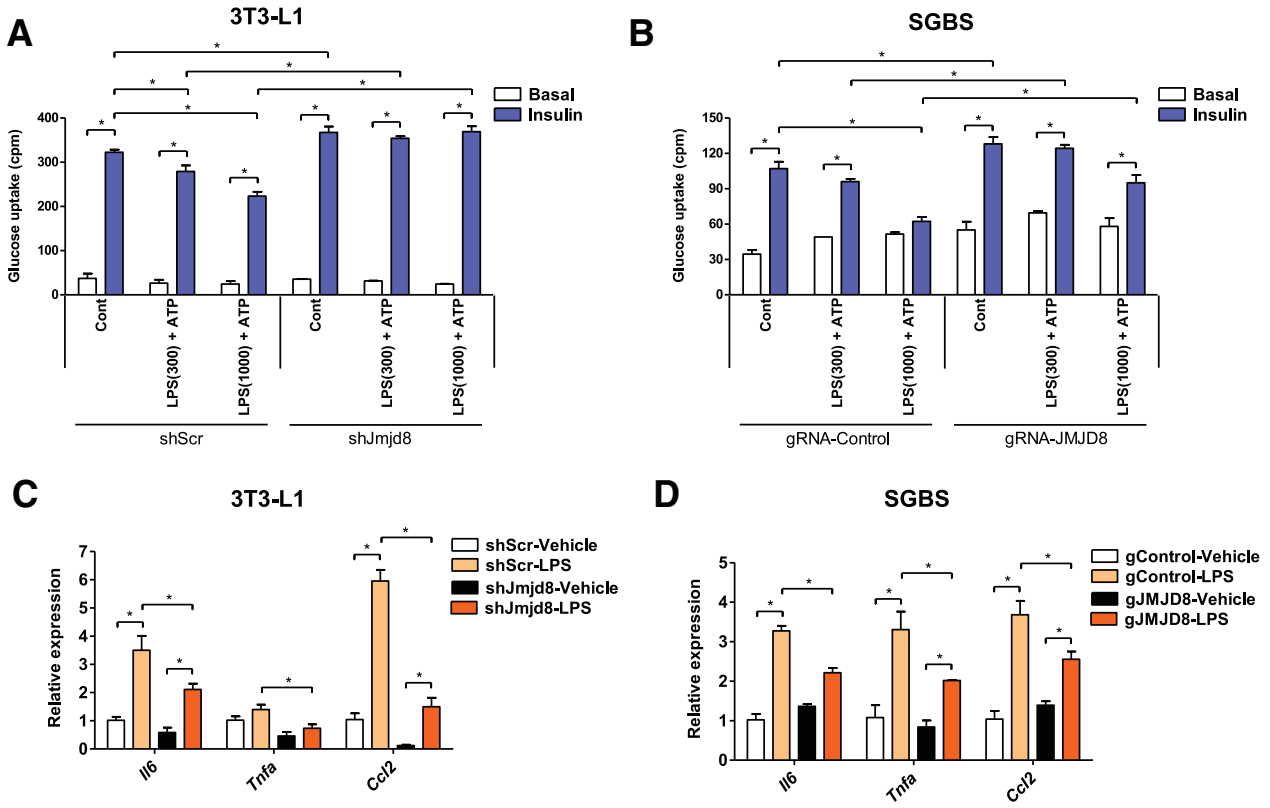

Figure 7—JMJD8 is required for the LPS-stimulated expression of inflammatory gene expression and insulin resistance. Mature 3T3-L1 adipocytes (*A*) or human SGBS adipocytes (*B*) were lentivirally infected with control shScramble (shScr) vs. hairpin against *Jmjd8* (shJmjd8) or control gRNA (gCont) vs. gRNA against *JMJD8* (gJMJD8) and treated with LPS (0, 300 or 1,000 ng/mL, 6 days) plus ATP (5 mmol/L, 6 h) or vehicle. Shown is the basal and insulin-stimulated glucose uptake measured by a ^{3}H-2-DG assay ($n = 4$; *$P < 0.05$, two-way ANOVA with Student *t* test, mean ± SEM). *C* and *D*: Cells from *A* and *B* were treated with LPS (10 μg/mL) plus ATP (5 mmol/L) or vehicle for 6 h. Shown is the qPCR measurement of the expression of inflammatory genes ($n = 3$; *$P < 0.05$, two-way ANOVA with Student *t* test, mean ± SEM). Cont, control.

we found that JMJD8 does not colocalize with Sec61, a channel protein located in the ER. This discrepancy might be ascribed to differences in the mouse and human orthologs between the studies.

The early events in the development of adipose inflammation are not well understood. One of the proposed mechanisms is that the innate immune pathways are directly activated by nutritional signals such as free fatty acids (52,53) and endotoxin (54). Indeed, there are pattern recognition receptors like TLR2 and TLR4 in adipocytes (24,26). The stimulation of TLR4 by LPS binding activates multiple signaling components, including NF-κB, AP-1, and IRF3, and causes the subsequent production of proinflammatory cytokines (54). Recent studies suggest that JMJD8 regulates the NF-κB pathway, but the results seem to be inconsistent. While two studies suggest that JMJD8 acts as a positive regulator of TNF-α–stimulated NF-κB signaling in HEK293T and colorectal cancer cell lines such as H1299 (55,56), another study reported that JMJD8 negatively regulates NF-κB activity in H1299 cells (57). In our studies, we noted that JMJD8 does not alter the canonical regulation of NF-κB, as evidenced by: *1*) the lack of clear changes in nuclear localization, *2*) similar levels of total and Ser536-phosphorylated NF-κB among obese *Jmjd8*-KO, *Jmjd8*-TG, and control eWAT, *3*) no physical interaction between JMJD8 and upstream regulators of NF-κB signaling, such as IκB or IKKβ, and *4*) the lack of effect on NF-κB–driven transcriptional activity.

The other arm of LPS-stimulated TLR signaling leads to the activation of IRF3 by inducing localization to the nucleus, where it acts as a transcription factor. Thus, we also examined the signaling arm of IRF3, finding a physical interaction between IRF3 and JMJD8 in 293T cells. Interestingly, we noted that IRF3 is important for JMJD8 activity, as evidenced by JMJD8 dramatically losing the ability to activate LPS-mediated inflammatory gene regulation and insulin resistance after losing IRF3. On the contrary, IRF3's actions were marginally affected when losing JMJD8. This arguably suggests that JMJD8 requires IRF3 to cause insulin resistance and inflammation, but not the reverse, at least in vitro. It is noteworthy that several functions for IRF3 have been reported in signaling within the cytoplasm, which are independent of its

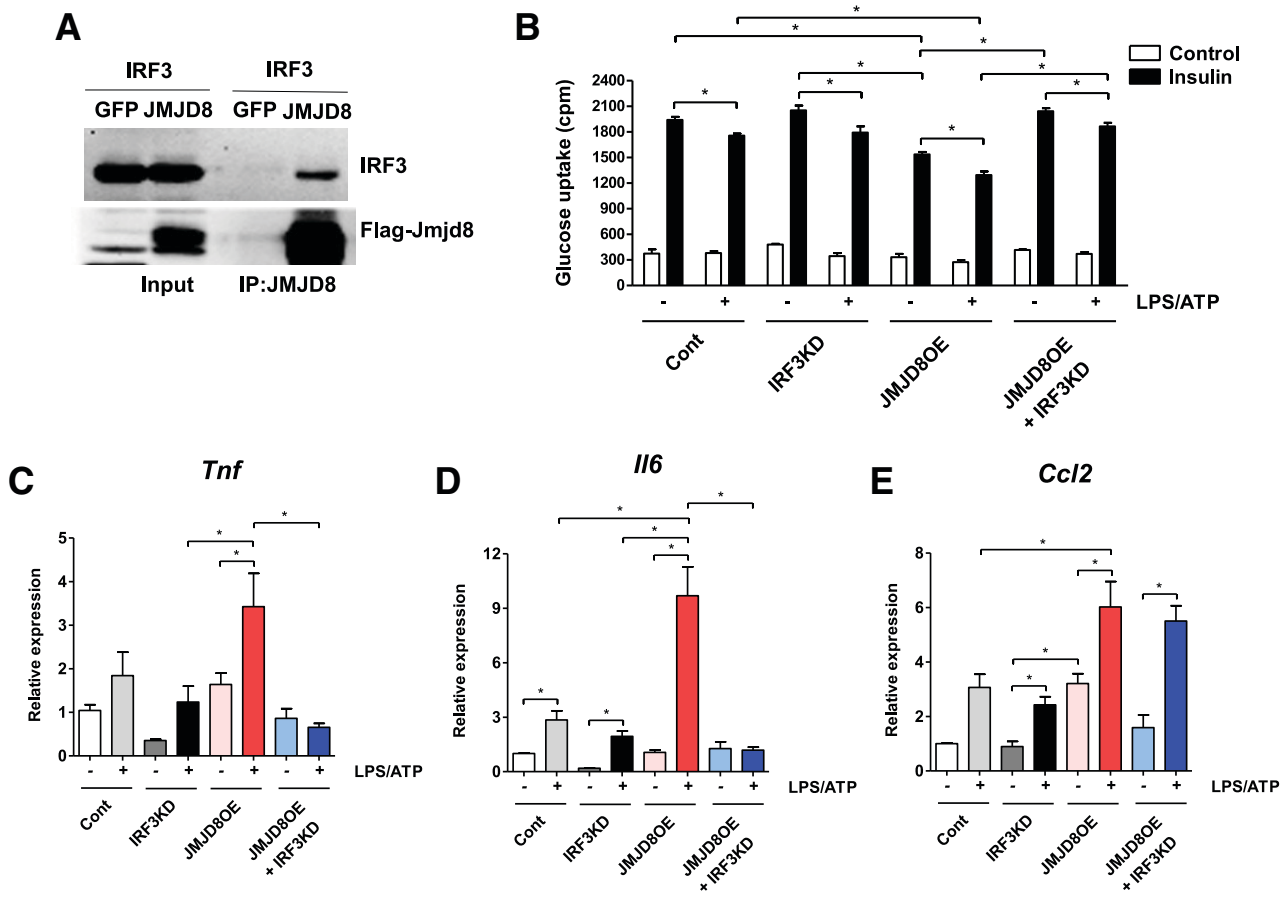

Figure 8—IRF3 is required for JMJD8 to mediate inflammatory gene regulation and insulin resistance. *A*: DNA plasmids expressing IRF3 and JMJD8 (or GFP) were transiently expressed in 293T cells, and cell lysates were immunoprecipitated (IP) with anti-JMJD8 and blotted for IRF3 or JMJD8. *B*: Basal and insulin-stimulated glucose uptake measured by a ^{3}H-2-DG assay in vehicle- or LPS-treated mature 3T3-L1 adipocytes that were infected with control vectors vs. gRNA against IRF3 (IRF3KD) and/or JMJD8 overexpressor (JMJD8OE) lentiviruses ($n = 4$; $^{*}P < 0.05$, two-way ANOVA with Student *t* test, mean ± SEM). *C–E*: qPCR analysis of *Tnf*, *Il6*, and *Ccl2* in cells from *B* ($n = 6$; $^{*}P < 0.05$, two-way ANOVA with Student *t* test, mean ± SEM). Cont, control.

nuclear function. For example, activated IRF3 inhibits TGF-β/Smad signaling (58), thus preventing the differentiation of induced regulatory T cells in colons and the epithelial-to-mesenchymal transition of tumor cells. A recent study also reported that IRF3 associates with active β-catenin in the cytoplasm, thus inhibiting its nuclear translocation and cell proliferation of colorectal tumor cells (59). Thus, it is possible that IRF3 regulates JMJD8 signaling in the cytoplasm. Future studies will be required to determine how IRF3 affects JMJD8-mediated LPS signaling.

Inflammatory signals negatively impact insulin signaling, for instance, by causing inhibitory serine phosphorylation at IRS1, which can lead to an increased IRS1 protein degradation (41–43). Consistent with this notion, *Jmjd8*-KO eWAT in high-fat–fed mice has greatly improved insulin signal transduction, caused reduced S612 phosphorylation of IRS1 and increased IRS1 protein levels, and, conversely, JMJD8-overexpressing adipocytes showed reduced insulin signal transduction. It is worth nothing that recent studies have indicated that JMJD8 regulates AKT signaling in cancer cell lines (57,60), although the results are opposing among the studies. Nevertheless, it appears that JMJD8 plays an important role in regulation of phosphorylation of AKT and other components of insulin signaling cascade. Whether this regulation is direct or indirect remains to be determined.

In summary, we identified JMJD8 as an important molecular regulator of inflammation and insulin sensitivity in adipocytes. Identifying the function of JMJD8 in adipose metabolic health may provide novel therapeutic targets for metabolic disorders including obesity and T2D.

Acknowledgments. The authors thank Dr. Evan Rosen (Harvard Medical School) for sharing the IRF3 overexpression plasmid and Drs. Hei Sook Sul, Jen-Chywan Wally Wang (University of California Berkeley), and Evan Rosen for helpful conversations about the manuscript.

Funding. Work was funded by American Heart Association award number 19POST34380834 to D.Y. and National Institute of Diabetes and Digestive and Kidney Diseases grant R01 DK116008 and Stanford Diabetes Research Center Pilot and Feasibility Program grant P30DK116074 to S.K.

Duality of Interest. No potential conflicts of interest relevant to this article were reported.

Author Contributions. S.K. supervised experiments and wrote the manuscript. D.Y. drafted the *Research Design and Methods* section and figure legends. Experiments were carried out by D.Y., B.C.J., S.D.V., and S.K. H.-W.L. analyzed RNA-seq. S.K. is the guarantor of this work and, as such, had full access to all of the data in the study and takes responsibility for the integrity of the data and the accuracy of the data analysis.

References

1. Saltiel AR, Olefsky JM. Inflammatory mechanisms linking obesity and metabolic disease. J Clin Invest 2017;127:1–4
2. Hotamisligil GS. Inflammation, metaflammation and immunometabolic disorders. Nature 2017;542:177–185
3. Lee YS, Wollam J, Olefsky JM. An integrated view of immunometabolism. Cell 2018;172:22–40
4. Schipper HS, Prakken B, Kalkhoven E, Boes M. Adipose tissue-resident immune cells: key players in immunometabolism. Trends Endocrinol Metab 2012;23:407–415
5. Molofsky AB, Nussbaum JC, Liang HE, et al. Innate lymphoid type 2 cells sustain visceral adipose tissue eosinophils and alternatively activated macrophages. J Exp Med 2013;210:535–549
6. Wu D, Molofsky AB, Liang HE, et al. Eosinophils sustain adipose alternatively activated macrophages associated with glucose homeostasis. Science 2011;332:243–247
7. Nussbaum JC, Van Dyken SJ, von Moltke J, et al. Type 2 innate lymphoid cells control eosinophil homeostasis. Nature 2013;502:245–248
8. Feuerer M, Herrero L, Cipolletta D, et al. Lean, but not obese, fat is enriched for a unique population of regulatory T cells that affect metabolic parameters. Nat Med 2009;15:930–939
9. Bapat SP, Myoung Suh J, Fang S, et al. Depletion of fat-resident Treg cells prevents age-associated insulin resistance. Nature 2015;528:137–141
10. Talukdar S, Oh DY, Bandyopadhyay G, et al. Neutrophils mediate insulin resistance in mice fed a high-fat diet through secreted elastase. Nat Med 2012;18:1407–1412
11. Winer S, Chan Y, Paltser G, et al. Normalization of obesity-associated insulin resistance through immunotherapy. Nat Med 2009;15:921–929
12. Nishimura S, Manabe I, Nagasaki M, et al. CD8+ effector T cells contribute to macrophage recruitment and adipose tissue inflammation in obesity. Nat Med 2009;15:914–920
13. Bertola A, Ciucci T, Rousseau D, et al. Identification of adipose tissue dendritic cells correlated with obesity-associated insulin-resistance and inducing Th17 responses in mice and patients. Diabetes 2012;61:2238–2247
14. Weisberg SP, McCann D, Desai M, Rosenbaum M, Leibel RL, Ferrante AW Jr. Obesity is associated with macrophage accumulation in adipose tissue. J Clin Invest 2003;112:1796–1808
15. Winer DA, Winer S, Shen L, et al. B cells promote insulin resistance through modulation of T cells and production of pathogenic IgG antibodies. Nat Med 2011;17:610–617
16. Lumeng CN, Bodzin JL, Saltiel AR. Obesity induces a phenotypic switch in adipose tissue macrophage polarization. J Clin Invest 2007;117:175–184
17. Hotamisligil GS, Shargill NS, Spiegelman BM. Adipose expression of tumor necrosis factor-alpha: direct role in obesity-linked insulin resistance. Science 1993;259:87–91
18. Feinstein R, Kanety H, Papa MZ, Lunenfeld B, Karasik A. Tumor necrosis factor-alpha suppresses insulin-induced tyrosine phosphorylation of insulin receptor and its substrates. J Biol Chem 1993;268:26055–26058
19. Cani PD, Amar J, Iglesias MA, et al. Metabolic endotoxemia initiates obesity and insulin resistance. Diabetes 2007;56:1761–1772
20. Creely SJ, McTernan PG, Kusminski CM, et al. Lipopolysaccharide activates an innate immune system response in human adipose tissue in obesity and type 2 diabetes. Am J Physiol Endocrinol Metab 2007;292:E740–E747
21. Dasu MR, Devaraj S, Park S, Jialal I. Increased toll-like receptor (TLR) activation and TLR ligands in recently diagnosed type 2 diabetic subjects. Diabetes Care 2010;33:861–868
22. Ghanim H, et al. Increase in plasma endotoxin concentrations and the expression of Toll like receptors and suppressor of cytokine signaling-3 in mononuclear cells after a high-fat, high-carbohydrate meal. Diabetes Care 2009;32:2281–2287
23. van der Crabben SN, Blümer RM, Stegenga ME, et al. Early endotoxemia increases peripheral and hepatic insulin sensitivity in healthy humans. J Clin Endocrinol Metab 2009;94:463–468
24. Shi H, Kokoeva MV, Inouye K, Tzameli I, Yin H, Flier JS. TLR4 links innate immunity and fatty acid-induced insulin resistance. J Clin Invest 2006; 116:3015–3025
25. Jialal I, Kaur H, Devaraj S. Toll-like receptor status in obesity and metabolic syndrome: a translational perspective. J Clin Endocrinol Metab 2014;99:39–48
26. Lin Y, et al. LPS activated TLR-4 receptor induces synthesis of the closely related receptor TLR-2 in adipocytes. J Biol Chem 2000;275: 24255–24263
27. Deng T, Lyon CJ, Minze LJ, et al. Class II major histocompatibility complex plays an essential role in obesity-induced adipose inflammation. Cell Metab 2013;17:411–422
28. Kumari M, Wang X, Lantier L, et al. IRF3 promotes adipose inflammation and insulin resistance and represses browning. J Clin Invest 2016; 126:2839–2854
29. Baker RG, Hayden MS, Ghosh S. NF-κB, inflammation, and metabolic disease. Cell Metab 2011;13:11–22
30. Kooistra SM, Helin K. Molecular mechanisms and potential functions of histone demethylases. Nat Rev Mol Cell Biol 2012;13:297–311
31. Abe Y, Fujiwara Y, Takahashi H, et al. Histone demethylase JMJD1A coordinates acute and chronic adaptation to cold stress via thermogenic phospho-switch. Nat Commun 2018;9:1566
32. Abe Y, Rozqie R, Matsumura Y, et al. JMJD1A is a signal-sensing scaffold that regulates acute chromatin dynamics via SWI/SNF association for thermogenesis. Nat Commun 2015;6:7052
33. Tateishi K, Okada Y, Kallin EM, Zhang Y. Role of Jhdm2a in regulating metabolic gene expression and obesity resistance. Nature 2009;458:757–761
34. Cheng Y, Yuan Q, Vergnes L, et al. KDM4B protects against obesity and metabolic dysfunction. Proc Natl Acad Sci USA 2018;115:E5566–E5575
35. Buerger F, Müller S, Ney N, et al. Depletion of Jmjd1c impairs adipogenesis in murine 3T3-L1 cells. Biochim Biophys Acta Mol Basis Dis 2017;1863:1709–1717
36. Oh S, Shin S, Janknecht R. The small members of the JMJD protein family: Enzymatic jewels or jinxes? Biochim Biophys Acta Rev Cancer 2019;1871:406–418
37. Dobin A, Davis CA, Schlesinger F, et al. STAR: ultrafast universal RNA-seq aligner. Bioinformatics 2013;29:15–21
38. Robinson MD, McCarthy DJ, Smyth GK. edgeR: a Bioconductor package for differential expression analysis of digital gene expression data. Bioinformatics 2010;26:139–140
39. Kuleshov MV, Jones MR, Rouillard AD, et al. Enrichr: a comprehensive gene set enrichment analysis web server 2016 update. Nucleic Acids Res 2016;44:W90–7
40. Wabitsch M, Brenner RE, Melzner I, et al. Characterization of a human preadipocyte cell strain with high capacity for adipose differentiation. Int J Obes Relat Metab Disord 2001;25:8–15

41. Yoneyama Y, Inamitsu T, Chida K, et al. Serine phosphorylation by mTORC1 promotes IRS-1 degradation through SCFβ-TRCP E3 ubiquitin ligase. iScience 2018;5:1–18
42. Lee YH, Giraud J, Davis RJ, White MF. c-Jun N-terminal kinase (JNK) mediates feedback inhibition of the insulin signaling cascade. J Biol Chem 2003;278:2896–2902
43. Aguirre V, Werner ED, Giraud J, Lee YH, Shoelson SE, White MF. Phosphorylation of Ser307 in insulin receptor substrate-1 blocks interactions with the insulin receptor and inhibits insulin action. J Biol Chem 2002; 277:1531–1537
44. Kang S, Kong X, Rosen ED. Adipocyte-specific transgenic and knockout models. Methods Enzymol 2014;537:1–16
45. Fitzgerald KA, Rowe DC, Barnes BJ, et al. LPS-TLR4 signaling to IRF-3/7 and NF-kappaB involves the toll adapters TRAM and TRIF. J Exp Med 2003;198:1043–1055
46. Freaney JE, Kim R, Mandhana R, Horvath CM. Extensive cooperation of immune master regulators IRF3 and NFκB in RNA Pol II recruitment and pause release in human innate antiviral transcription. Cell Rep 2013; 4:959–973
47. Wietek C, Miggin SM, Jefferies CA, O'Neill LAJ. Interferon regulatory factor-3-mediated activation of the interferon-sensitive response element by Toll-like receptor (TLR) 4 but not TLR3 requires the p65 subunit of NF-κ. J Biol Chem 2003;278:50923–50931
48. Osborn O, Olefsky JM. The cellular and signaling networks linking the immune system and metabolism in disease. Nat Med 2012;18:363–374
49. Huang Y, Chen D, Liu C, Shen W, Ruan Y. Evolution and conservation of JmjC domain proteins in the green lineage. Mol Genet Genomics 2016;291:33–49
50. Khoueiry R, Sohni A, Thienpont B, et al. Lineage-specific functions of TET1 in the postimplantation mouse embryo. Nat Genet 2017;49:1061–1072
51. Yeo KS, Tan MC, Lim Y-Y, Ea C-K. JMJD8 is a novel endoplasmic reticulum protein with a JmjC domain. Sci Rep 2017;7:15407
52. Huang S, Rutkowsky JM, Snodgrass RG, et al. Saturated fatty acids activate TLR-mediated proinflammatory signaling pathways. J Lipid Res 2012;53:2002–2013
53. Pal D, Dasgupta S, Kundu R, et al. Fetuin-A acts as an endogenous ligand of TLR4 to promote lipid-induced insulin resistance. Nat Med 2012;18:1279–1285
54. Pålsson-McDermott EM, O'Neill LAJ. Signal transduction by the lipopolysaccharide receptor, Toll-like receptor-4. Immunology 2004;113: 153–162
55. Yeo KS, Tan MC, Wong WY, et al. JMJD8 is a positive regulator of TNF-induced NF-κB signaling. Sci Rep 2016;6:34125
56. Boeckel J-N, Derlet A, Glaser SF, et al. JMJD8 regulates angiogenic sprouting and cellular metabolism by interacting with pyruvate kinase M2 in endothelial cells. Arterioscler Thromb Vasc Biol 2016;36: 1425–1433
57. Su Y, Wang J. JmjC domain-containing protein 8 (JMJD8) represses Ku70/Ku80 expression via attenuating AKT/NF-κB/COX-2 signaling. Biochim Biophys Acta Mol Cell Res 2019;1866:118541
58. Xu P, Bailey-Bucktrout S, Xi Y, et al. Innate antiviral host defense attenuates TGF-β function through IRF3-mediated suppression of Smad signaling. Mol Cell 2014;56:723–737
59. Tian M, Wang X, Sun J, et al. IRF3 prevents colorectal tumorigenesis via inhibiting the nuclear translocation of β-catenin. Nat Commun 2020; 11:5762
60. Zhang B, Zhang Y, Jiang X, et al. JMJD8 promotes malignant progression of lung cancer by maintaining EGFR stability and EGFR/PI3K/AKT pathway activation. J Cancer 2021;12:976–987